Milli-PIV rheology of shear-thinning fluids

M. Chinaud [a], T. Delaunay [a], S. Cazin [b], E. Cid [b], Ph. Tordjeman [b,*]

[a] Laboratoire IES, Groupe Micro et RhéoAcoustique, UMR CNRS 5214, Université Montpellier 2, CC 082, Pl. E. Bataillon, 34095 Montpellier Cedex 05, France
[b] Université de Toulouse, INPT – CNRS, Institut de Mécanique des Fluides de Toulouse (IMFT), 1 Allée du Professeur Camille Soula, 31400 Toulouse, France

A B S T R A C T

Milli-Particle Image Velocimetry (Milli-PIV), which is an application of the standard PIV has been developed to measure the velocity distribution of complex fluids in a millimetric Hele-Shaw cell. A laser sheet is sent perpendicularly to the cell and the camera observes the PIV images via an internal optical prism. We studied, with Milli-PIV, a structural series of shear thinning xanthan fluids at different injection rates. We determined the velocity profiles in the thickness of the flow cell and discussed the accuracy of measurement. Using an inverse method, we calculated the constitutive parameters and showed that they are similar to those measured by rheology. The pressure gradient characteristic of the couple experimental conditions – fluid were also calculated from modeling the velocity profile.

Keywords:
Milli-PIV
Shear thinning fluids
Hele-Shaw cell
Velocity profile

1. Introduction

The rheology of complex fluids has been the subject of attention for decades, partly in relation to its relevance not only in processing or commercial applications but also for fundamental research. Recent studies have pointed out that nonlinear behaviors may be related to the heterogeneous nature of the flow. Experiments showed that complex fluids could exhibit wall-slip [1], shear banding [2,3], elastic shear thinning instability [4], "spurt" effect [5] or many other instabilities linked to their constitutive law [6]. Furthermore, for wormlike micellar solutions, the shear-induced microstructure can induce shear-induced phase separation [7,8]. If recent models have been proposed to understand the relationship between the nature of the instability and the constitutive equation [4,9–12], the flow microstructures have been pointed out by coupling the rheological measurements with a microstructural characterization technique. A large number of techniques have been used to characterize the flow heterogeneities at different scales. One can quote for instance small-angle neutron scattering [7,13], ultrasonic speckle velocimetry [14], nuclear magnetic resonance microscopy [5], birefringence measurements [15].

For the moderately turbid complex fluids, we suggest an alternative strategy based on Particle Image Velocimetry (PIV) to characterize the velocity distribution in a flow cell. Indeed, the direct observation of the velocity profile would reveal whether or not there is a flow instability. Furthermore, the assumption of a constitutive equation could be validated by comparing the experimental velocity profile with that computed from the constitutive relation. This approach allows a constitutive equation of a complex fluid to be tested over a very large range of shear rate (up to $10^4\ s^{-1}$).

In this paper, we will show the possibility to characterize the flow of complex fluids by PIV in a millimetric Hele-Shaw cell. First, we will study the stable flow of a structural series of model shear thinning fluids in order to validate the experimental procedure. Then, following an inverse approach, we will establish that the constitutive equations of the complex fluids determined from the PIV measurements are identical to those obtained from the rheological experiments. This work is the first step to study the flow instabilities of complex fluids by PIV.

In conventional PIV [16–18], the velocity of a fluid is measured throughout a region illuminated by a 2D laser light sheet. "Seeding" flow following particles are introduced into the flow and their motion is used to quantify the velocity of the local fluid. The particles are chosen to be as far as possible, neutrally buoyant, chemically inert and with optimized optical properties. The particle images are recorded during the flowing time using a digital camera. Each image is divided in "interrogation windows". The displacement of the particle patterns between consecutive images and for a given interrogation window is obtained from the peak position in the 2D cross-correlation plane of the two consecutive images. Finally, the particle velocities in the light sheet are simultaneously calculated from the value of the displacement and the time delay between two laser pulses. Over the past decade, PIV has undergone significant improvements. From a theoretical point of view, new "interrogation algorithms" had been developed giving an accuracy of synthetic images from Monte Carlo simulations close to 0.01 pixel [19,20]. Recently, Westerweel [21] proposed a

* Corresponding author. Tel.: +33 5 34 32 28 58.
E-mail address: philippe.tordjeman@imft.fr (Ph. Tordjeman).

model to take into account the effects of local velocity gradients on the PIV accuracy. He showed that the random error is proportional to the width of the displacement-correlation peak which is a square root function of the shear rate. In this work, the effects of the velocity gradients were studied at the scale of the interrogation window. They must be considered only if the following criterion is satisfied [22]: $\frac{\partial v}{\partial x}\Delta t > \frac{d_\tau}{L}$, where $\frac{\partial v}{\partial x}$ is the velocity gradient, Δt is the exposure time delay, L is a characteristic interrogation window length and d_τ is the particle image diameter.

From an experimental point of view, the achievable accuracy of the PIV measurements is of the order of 0.1 pixel [23] and is limited by the variation of particle image intensities [19].

One can distinguish two experimental limit configurations in the 2D PIV measurements: the first corresponds to the conventional case where the depth of field of the optical lens – camera system is higher than the thickness of the light sheet [24]; the second corresponds to the case where the depth of field is lower than the thickness of the light sheet. This configuration had allowed the development of the μPIV [1,25–29] for which the velocity field in a microfluidic device is measured by the whole illumination of the liquid in flow. The intermediate case called Milli-PIV where the depth of field is of the same order of the thickness of the light sheet and close to the typical length of flow has rarely been studied. The Milli-PIV configuration is of a great interest for our study because it allows characterizing the flow of complex fluids in a large range of shear rates and with reliable large and instantaneous velocity fields in comparison with μPIV. It is an application of the standard PIV that allows studying flows in millimeter confined geometry.

2. Model complex fluids

Dilute solutions of xanthan gum were prepared by dissolving appropriate amounts of polymer in distilled water. Xanthan gum ($C_{35}H_{49}O_{29}$) is a natural polysaccharide commonly used in the food industry. It consists of long-chain molecules of high molecular weight ($Mn = 3 \times 10^6$ g/mol). This bio-polymer is soluble in water at room temperature for a large pH range. Six different concentrations of xanthan gum were made and varied between 100 and 2500 ppm in xanthan gum (Table 1). Previous experiments showed that the volume weights at room temperature for this range of concentrations are nearly-independent of the amount of polymer ($\rho = 998.5$ kg m^{-3}) [30]. The fluids were prepared just before each trial of rheological experiments or Milli-PIV experiments.

The solutions of the xanthan gum exhibit a shear thinning behavior which corresponds to a strong shear rate dependence of the viscosity. Changing the concentration allows us to modify the rheological behavior from weak shear thinning for low concentrations to strong shear thinning for high concentrations. The shear rate dependence of the viscosity was measured for the six solutions at 20 °C using a stress rheometer (Rheometric Scientific ARES 2000) in the Couette geometry. The range in shear rate is limited at the low values by the sensitivity of the stress transducer and at the high values by the appearance of the Taylor–Couette instability. There are no measurable normal stresses for the xanthan concentrations defined in this study. Graphs of the viscosity versus the shear rate are shown in Fig. 1. In the shear thinning zone, these curves could be fitted by the well-known power-law:

$$\eta(\dot{\gamma}) = K\dot{\gamma}^{n-1}, \tag{1}$$

where η and $\dot{\gamma}$ are the shear viscosity and the shear rate, respectively. The Fig. 1 displays that the power-law model is relevant for a shear rate higher than $\dot{\gamma}_L = 10$ s^{-1} for all the xanthan solutions. The corresponding constitutive parameters (n, K) are listed in Table 1, n being the pseudoplastic index ($n < 1$) and K the flow consistency index. The standard deviation estimated from the rheological measurements is ±10% for n and ±15% for K. For this series of xanthan solutions, we show in Fig. 2 that the flow consistency index is determined by the pseudoplastic index and follows a semi-logarithmic relationship: $n = 0.993 - 0.100 \ln K$. This curve is obtained from the n and K values measured in this study and those of the literature collected in Table 1 [30,31]. The latter clearly shows that the n and K values measured by rheology are scattered in the literature. This can be understood by considering that the rheological behavior is function of the weight distribution of the polymer, of the method of formulation, of the rheometer calibration and of the aging of the complex fluids.

For PIV experiments, the xanthan fluids are considered as "difficult" because they present important shear rates close to the wall compared with Newtonian fluids. Furthermore, the turbidity increases with the amount of diluted polymer. One can note that the fluids with a low concentration of xanthan (lower than 250 ppm) are Newtonian-like.

3. Milli-PIV experiment

A flow channel was built consisting of an injection jack fixed on uniaxial displacement controller and connected to a milli-channel (Fig. 3a). The injection jack diameter is 36 mm and its length is 254 mm. The uniaxial displacement controller can move the piston with a speed V_p between 10 μm s^{-1} and 500 mm s^{-1}. The corresponding flow rate can change between 1×10^{-8} and 5×10^{-4} m^3 s^{-1}. The speed is interlocked by a Servostar 300 controller driven by a specific Labview program. A 5 l tank that contains the studied fluid is placed above the injection jack. The latter is simply filled with the fluid by gravity, a draining system provides an air vent. The fluid is pushed from the injection jack to the milli-channel via a flexible tube, which has a diameter of 10 mm. It assures that there is no movement transmitted to the channel during the exper-

Table 1
Constitutive parameters n and K of Eq. (1) measured by rheology: data of this work and of the literature [30,31].

Concentration (ppm)	K (mPa s^n) ± 15%	n ± 10%	K (mPa s^n) from [31]	n from [31]	K (mPa s^n) from [30]	n from [30]
5000	4331.6	0.23	/	/	/	/
3000	/	/	1089	0.27	/	/
2500	409.3	0.45	/	/	/	/
2000	/	/	568	0.33	/	/
1750	/	/	511	0.33	/	/
1500	100.7	0.57	/	/	/	/
1250	86.4	0.59	/	/	/	/
1000	/	/	160	0.46	138	0.46
500	19.3	0.73	41	0.61	53	0.55
250	5.4	0.89	11	0.73	24	0.62
200	5	0.92	11	0.74	/	/
100	3	0.97	5	0.82	15	0.67
50	/	/	/	/	7	0.76

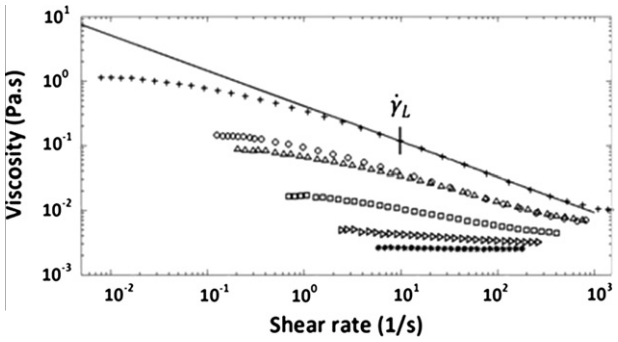

Fig. 1. Viscosity versus the shear rate for the 2500 ppm (+), 1500 ppm (○), 1250 ppm (Δ), 500 ppm (□), 250 ppm (▷) and 100 ppm (∗) xanthan fluids. $\dot{\gamma}_L = 10\ s^{-1}$ is the critical shear rate above which the power-law is valid for all xanthan solutions.

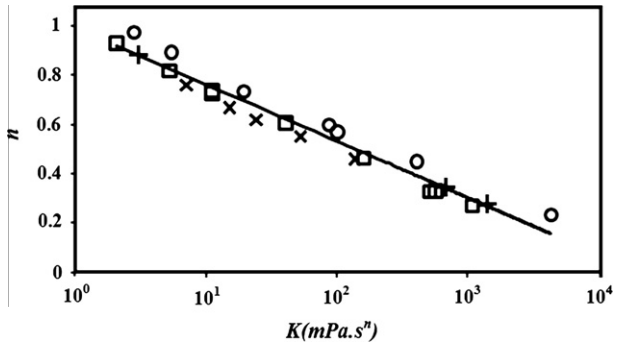

Fig. 2. Semi-logarithmic relationship between the constitutive parameters n and K of Eq. (1) plotted from the experimental data of this work and of the literature ((×) [30] and (□) [31]). (+) indicate the constitutive parameters obtained from the fit of velocity profiles.

iment. We have verified that the pressure losses are negligible for this tube.

The milli-channel is a Hele-Shaw cell and consists of two sheets of glass that measure 19 × 300 × 90 mm. The two sheets are separated by a distance of b = 5 mm and are maintained together by a specific aluminum. The parallelism bias between the two glass sheets measured by reflection of ultrasonic waves is lower than 100 μm. The water tightness is assured by a rubber toric seal. The inside flowing width is w = 50 mm. For this geometry where $b/w = 0.1$, the flow is unidirectional and the velocity $\vec{v}(z,n,K)$ is only a function of the thickness z. In these conditions and when the shear viscosity of the fluid follows the power law (Eq. (1)), it is possible to calculate the complete expression of the velocity as a function of the constitutive parameters:

$$\vec{v}(z,n,K) = \frac{n}{n+1}\left(\frac{1}{K}\frac{\partial P}{\partial x}\right)^{1/n}\left(z^{n+1/n} - \left(\frac{b}{2}\right)^{n+1/n}\right), \tag{2}$$

where $\frac{\partial P}{\partial x}$ is the pressure gradient. The corresponding flow rate is:

$$Q(n,K) = \frac{2n}{2n+1}\left(\frac{1}{K}\frac{\partial P}{\partial x}\right)^{1/n}\left(\frac{b}{2}\right)^{2n+1/n}. \tag{3}$$

For the Milli-PIV measurements, a Quantel Twin Ultra Nd: YAG laser of 2 × 30 mJ generates a light sheet (λ = 532 nm) by means of optical lens. The light sheet is sent perpendicularly to the glass sheet in the middle of the cell (Fig. 3b). We placed a little 45° reflected prism with a height of 5 mm (from Edmund Optics) in the wall to avoid any perturbation in the flow. The thin reflected layer deposed on the prism surface is in enhanced aluminum and its thickness is constant with a precision close to $\lambda/8$, where λ is the light wave length. In this case, a PCO Sensicam 12-bits CCD camera (1280 × 1024 pixel^2) is fixed perpendicularly to the glass sheet and just above the little prism (f = 105 mm, NA = 11, M = 0.83). The camera aperture and the depth of field were defined to record the displacement of the illuminated tracers with a maximum of sharpness. Under this condition the minimum value of the depth of field is close to 300 μm. This value was estimated on the base of a circle of confusion of 1 pixel. The camera is also equipped with a 540-nm high-pass filter.

The tracers are fluorescent polymethyl methacrylate (PMMA) particles that contain encapsulated B-Rhodamine (Dantec Dynamics). Their size distribution, measured with a Malvern Mastersizer granolumeter, is Gaussian and the mean diameter is around 10 μm. When the tracers are excited by the laser, the peak fluorescence of B-Rhodamine is located at approximately 570 nm. The high pass filter, placed in the camera viewing axe, prevents laser light transmission, but permits fluorescent light emitted by seeding particles to be collected. The shear thinning solutions were prepared with a particle concentration of 0.004% (w/w). The sedimentation velocity of the particles is around 20 μm/s [32] that is much smaller than the characteristic flow velocities.

Image pairs were captured from the CCD camera, which is synchronized with the laser. Time separation between two close consecutive pulses was set according to the flow velocity under investigation. We checked that the optical index of all the solutions does not change significantly because the focus on particles remains unchanged for different solution concentrations in xanthan gum. Although the turbidity increases with the amount of diluted polymer, the images stay exploitable for all the polymer concentrations (Fig. 3b inset).

In order to calculate the 2D velocity field $\vec{v}(z,n,K)$, we used the PIVIS software, which is an in-house competence developed by the Institut de Mécanique des Fluides de Toulouse. The algorithm is based on a 2D FFT cross-correlation function implemented in a multi-pass iterative scheme with a sub-pixel image deformation PIV [33,34]. Cross-correlation analysis of double particle images were carried out for three sizes of the interrogation windows: 64 × 64 pixels^2, 32 × 32 pixels^2 and 16 × 16 pixels^2 with an overlapping of 50%. Here, the objective was to optimize the accuracy of our Milli-PIV measurements and to verify that there was no peak locking. Moreover, we checked that planar deformation method does not modify the displacement correlation peaks (the sharp main correlation peaks emerge clearly from the secondary peaks with lower amplitude) and then, the calculated velocity field. For all the experiments, the same post processing was used to reject outliers. In particular, spurious vectors in region external to the cell were not eliminated even if they represent unphysical data.

To calibrate the velocity field, we machined a calibration target. This target was introduced in the channel filled by solution and images were recorded in the setting Milli-PIV conditions in the same plan as the laser sheet.

4. Results

By Milli-PIV, we studied at 20 °C three complex fluids (200 ppm, 1250 ppm and 2500 ppm xanthan fluids) at different velocities of the injection jack: 10, 30 and 50 mm s^{-1}. For each velocity, we recorded 40 double images. We calculated the mean velocity fields in the space 992 × 800 pixels^2. The Fig. 4 shows an example of a 3D representation of the velocity field in the thickness for the 1250 ppm xanthan fluid at 10 mm s^{-1}. The 40 velocity profiles corresponding to the 992 pixels distance are averaged, filtered and yields to a unique profile characteristic of the fluid for a given flow rate. We clearly observe in Fig. 4 on the right that the prism was dirtied by tracers near its base. Unfortunately, this was always observable with the fluids of higher viscosity. This effect causes a

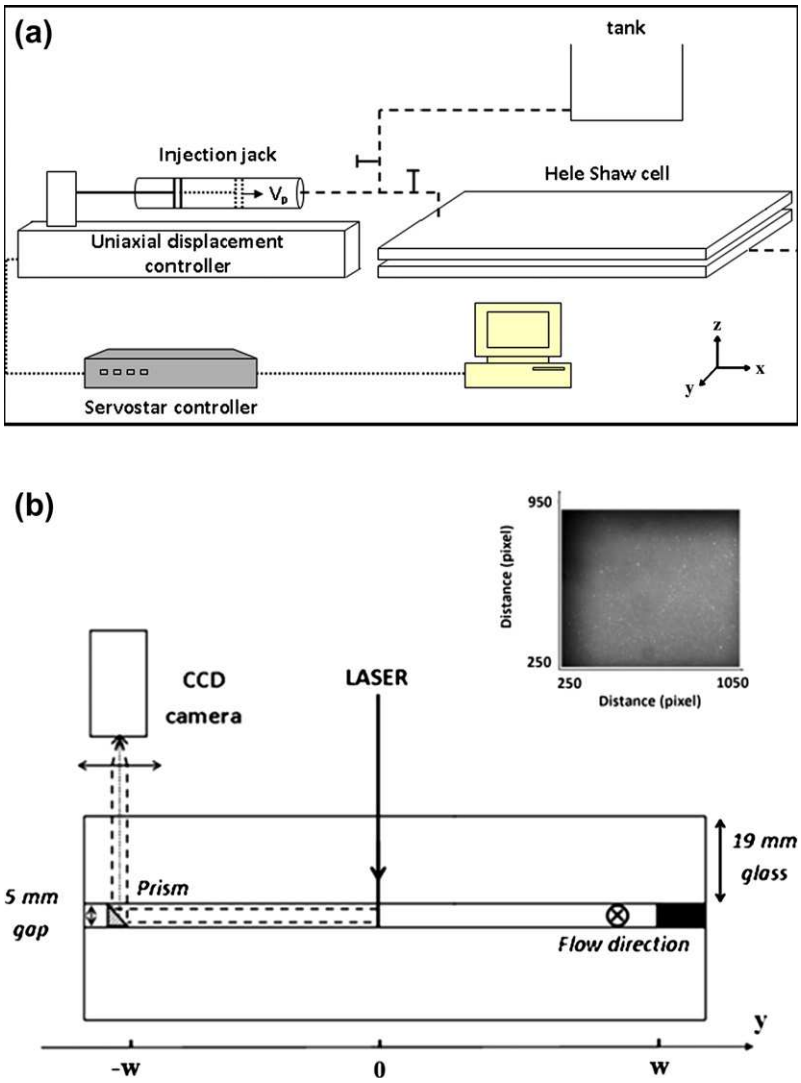

Fig. 3. (a) Schema of the experimental device. The dimensions of the flow channel are 19 × 300 × 90 mm, (b) Milli-PIV configuration: the solid line represents the optical trajectory of the laser sheet and the dashed lines represent the optical camera field. Inset: example of a Milli-PIV image for high turbid polymer solution (1250 ppm xanthan fluid). $-w$ and w indicate the position of the walls.

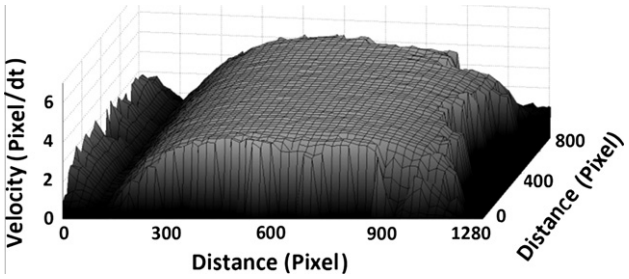

Fig. 4. 3D velocity representation of the 1250 ppm xanthan fluid measured by Milli-PIV. The velocity injection is 10 mm/s.

dissymmetry in the mean velocity profile. It is due to the fact that we did not have the possibility to clean up the prism between each trial. On the other hand, we never observed any specular reflection of laser light.

The velocity profiles of the fluids with 200 ppm and 1250 ppm in xanthan for different flow rates are presented in Figs. 5 and 6. We observe that the two fluids exhibit a different rheological behavior, as expected. Indeed, the 200 ppm xanthan fluid is Newtonian-like and the velocity profiles have a parabolic form in a first approximation. On the other hand, the 1250 ppm xanthan fluid is pseudoplastic and the velocity profiles are similar to that of a plug flow with high shear rates close to the walls. These curves clearly show that the maximum velocities increase with the injection flow rate. Figs. 7 and 8 compare the velocity profile of the 200 ppm and the 2500 ppm xanthan solutions at 30 and 50 mm/s. They present the viscosity effect in the velocity profile and show that the maximum velocities at a given flow rate decrease with the Newtonian zero-shear viscosity of the fluids.

We studied the accuracy of the Milli-PIV experiments. For the three xanthan fluids, the highest values of the velocity gradients $\frac{\partial v}{\partial x}$, localized close to the walls, are around 300 s^{-1} at an injection velocity of 50 mm/s (Fig. 9). We verified that: $\frac{\partial v}{\partial x}\Delta t < \frac{d_\tau}{L}$, where the time delay $\Delta t = 306$ μs, the interrogation window length $L = 243$ μm and the image particle diameter $d_\tau = 25$ μm. This result allows us to disregard the shear rate effects of our measurements. In addition, we can neglect the velocity gradient effects in the depth of the interrogation volume window because the ratio of the laser sheet thickness to the cell width is around 0.02. We verified that, in the limit of the error bars, the velocity gradient curve of the 200 ppm xanthan fluid is linear in the cell thickness, as expected for Newtonian fluid (Fig. 9).

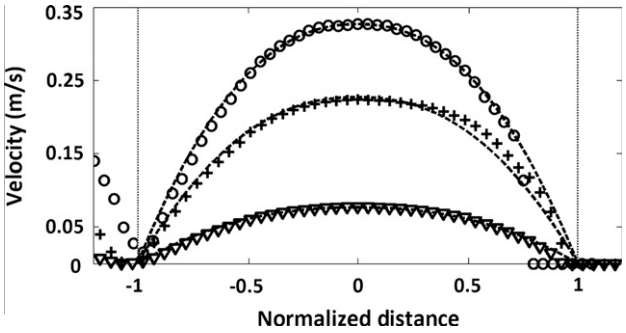

Fig. 5. Velocity profiles of the 200 ppm xanthan solution by Milli-PIV. The injection velocities are 50 mm/s (○), 30 mm/s (+) and 10 mm/s (▽). The distance is normalized by the cell thickness $b = 5$ mm. The dotted lines represent the walls of the Hele-Shaw cell. The dashed lines represent the power law velocity fits for $n = 0.9$.

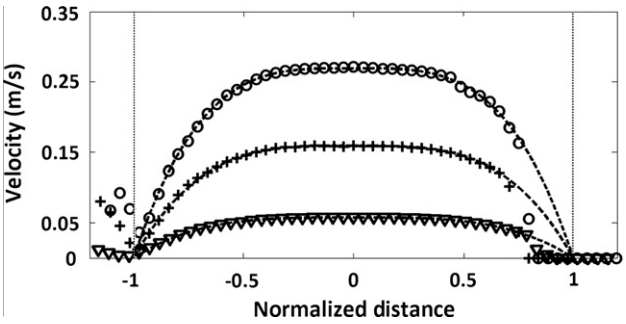

Fig. 6. Velocity profiles of the 1250 ppm xanthan solution by Milli-PIV. The injection velocities are 50 mm/s (○), 30 mm/s (+) and 10 mm/s (▽). The distance is normalized by the cell thickness $b = 5$ mm. The dotted lines represent the walls of the Hele-Shaw cell. The dashed lines represent the power law velocity fits for $n = 0.4$.

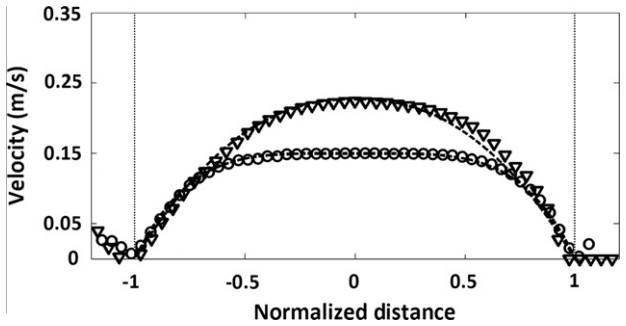

Fig. 7. Velocity profiles of the 2500 ppm (○) and 200 ppm (▽) xanthan solutions at an injection velocity of 30 mm/s by Milli-PIV. The distance is normalized by the cell thickness $b = 5$ mm. The dotted lines represent the walls of the Hele-Shaw cell. The dashed lines represent the power law velocity fits for $n = 0.3$ and $n = 0.9$.

Fig. 10 shows the mean velocity and the standard deviation versus the number of velocity profiles for the 2500 ppm xanthan fluid. If we consider that a constant mean velocity is obtained after 18 velocity profiles, the standard deviation reaches a constant value around $\sigma \approx 0.20$ pixel/s. The standard deviations calculated for each experimental condition are collected in Table 2.

Following an inverse approach, we fitted all the velocity profiles measured with Milli-PIV for $\frac{\partial v}{\partial x} \geq \dot{\gamma}_L$ by the Eq. (2) in order to determine the constitutive parameters n and K. More precisely, the n value is determined from the experimental profiles using the least-squares method. The corresponding K value is obtained from the master curve of Fig. 2. Furthermore, it is possible to determine

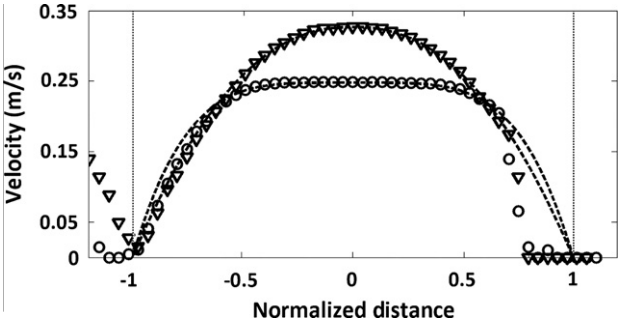

Fig. 8. Velocity profiles of the 2500 ppm (○) and 200 ppm (▽) xanthan solutions at an injection velocity of 50 mm/s by Milli-PIV. The distance is normalized by the cell thickness $b = 5$ mm. The dotted lines represent the walls of the Hele-Shaw cell. The dashed lines represent the power law velocity fits for $n = 0.3$ and $n = 0.9$.

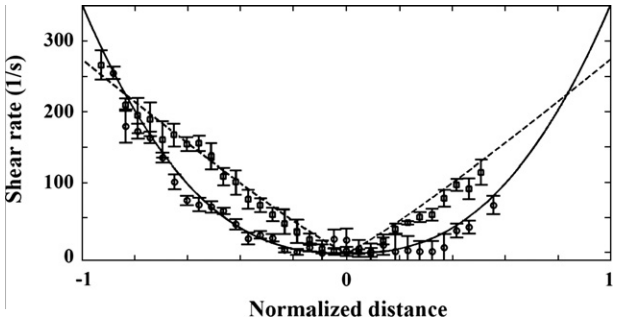

Fig. 9. Shear rate profile in the cell thickness for 200 ppm (□) and 1250 ppm (○) xanthan fluids. The distance is normalized by the cell thickness $b = 5$ mm. The injection velocity is 50 mm/s. The dashed line represents the theoretical shear rate for $n = 0.9$ and the solid line for $n = 0.4$.

from the fits the pressure gradient, $\frac{\partial P}{\partial x}$, characteristic of the experiments. All the data obtained from the minimization were collected in Table 2. One can note that the constitutive parameters calculated by inverse method for the same fluid are identical whatever injection rate. We verified for each case, that the injection flow rate is equal to the flow rate in the channel calculated from the velocity profile. In another way, we can check the mass conservation by plotting the $\frac{\partial P}{\partial x}$ coefficients versus injection velocity power n. We found that these two parameters are proportional with a coefficient characteristic of the fluid, according to the Eq. (3). The fits are presented in Figs. 5–8 and are in a good agreement with the experimental profiles.

One can observe that the constitutive parameter n obtained from the fitted velocity curves (Table 2) is always lower than those

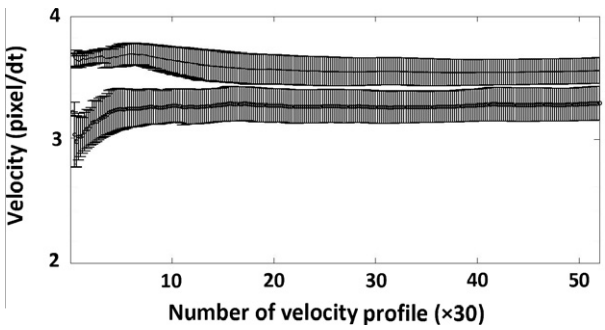

Fig. 10. Mean velocity and standard deviation versus the number of velocity profiles for 2500 ppm xanthan solution, at the center of the channel (large values of the velocity) and close to the wall of the channel (low values of the velocity).

Table 2
Constitutive parameters n and K of Eq. (1) and pressure gradient calculated by inverse method and experimental standard deviation of the velocity σ measured by Milli-PIV. The K and $\frac{\partial p}{\partial x}$ values were obtained for the mean n values. V_p is the speed of the piston.

Complex fluids	Vp (mm/s)	$\frac{\partial p}{\partial x}$ (mPa/m)	σ (mm/s)	n	K (mPa s^n)
200 ppm	10	52	2.9	0.9 ± 0.1	3
	30	137	8.3		
	50	159	8.3		
1250 ppm	10	885	8.3	0.40 ± 0.08	473
	30	1243	8.3		
	50	1537	9.0		
2500 ppm	30	2546	8.3	0.30 ± 0.05	1019
	50	2955	5.7		

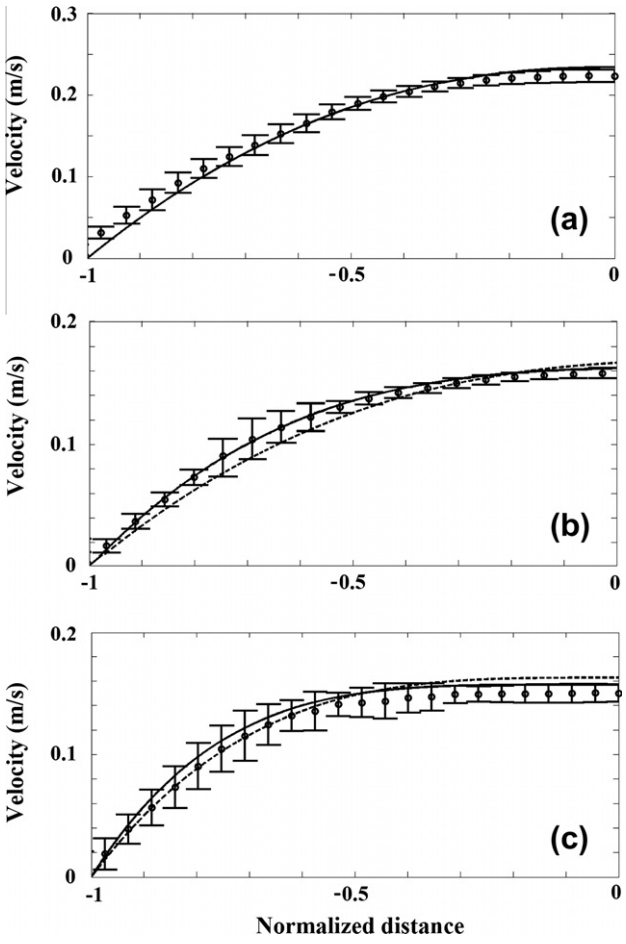

Fig. 11. Half-velocity profiles for an injection velocity of 30 mm/s. For the 200 ppm xanthan solution (a), the solid line represents the power-law velocity profile for $n = 0.9$. For the 1250 ppm xanthan solution (b), the solid line represents the power-law velocity profile for $n = 0.4$ and the dashed line for $n = 0.6$. For the 2500 ppm xanthan solution (c), the solid line represents the power-law velocity profile for $n = 0.3$ and the dashed line for $n = 0.45$.

obtained from with rheological measurements (Table 1). However, the Fig. 11, which compares the experimental velocity fields to those computed with the constitutive parameters calculated from the fit and measured by rheology, shows that the velocity profiles are similar. Indeed, for $\frac{\partial v}{\partial x} \geqslant \dot{\gamma}_L$ and in the limit of the accuracy, we observe a good agreement between experimental data and the model velocity profiles for each (n, K) value couple. One can note that the constitutive parameters summarizing in Table 2 present a best qualitative agreement with the complete velocity profile (Figs. 5–8). Thus, we show that the Milli-PIV results are in agreement with those measured by rheology.

5. Conclusion

We developed experiments to study the flow behavior of complex fluids by Milli-PIV. The experimental set up is constituted by a millimetric Hele-Shaw cell coupled to an injection jack. A small 45° prism inserted in the Hele-Shaw was used to characterize the velocity distribution in the thickness of the flow cell by PIV: a 2D laser sheet was sent perpendicularly to the cell and parallel to the flow direction. The PIV images acquisition were realized using the internal optical prism. Under these conditions, the depth of field of the optical lens-camera system is of the same order of magnitude as the laser sheet thickness and the Hele-Shaw cell thickness.

We studied a structural series of shear thinning xanthan fluids. For a small amount of polymer, the fluids are Newtonian-like and the velocity profiles measured by Milli-PIV display an expected parabolic form. For a large amount of polymer, the fluids are pseudoplastic and the velocity profiles exhibit a plug flow form. We showed that the velocity standard deviation is not affected by the shear rate and is close to $\sigma \approx 0.20$ pixel/s. A good accuracy of Milli-PIV could be expected for the large Δt values. However, Δt is limited by the displacement of the seeding particles between two consecutive images. Unfortunately, the experiments pointed out that a small deposit of tracers on the internal prism affects the quality of the measurements and is responsible for a dissymmetry in the velocity profile.

Considering that the shear rate dependence of the viscosity can be modeled by a power law $\eta(\dot{\gamma}) = K\dot{\gamma}^{n-1}$, we calculated the constitutive parameters n and K from the experimental profiles by an inverse method. For a given fluid, all the velocity profiles obtained at different injection rates yield the same couple of constitutive parameters. Furthermore, in the limit of the accuracy for the rheological experiments, we showed that the constitutive parameters determined using inverse method are similar to those measured by rheology. Finally, by fitting the velocity profiles, we estimated the pressure gradients characteristic of the experiments.

This work is the first step to study the flow stability of complex fluid by Milli-PIV. It will allow understanding of the relationship between the nature of instability and the constitutive equation of complex fluids.

References

[1] G. Degré, P. Joseph, P. Tabeling, et al., Rheology of complex fluids by particle image velocimetry in microchannels, Appl. Phys. Lett. 89 (2006) 24104–24107.
[2] J.B. Salmon, L. Bécu, S. Manneville, A. Colin, Towards local rheology of emulsions under Couette flow using dynamic light scattering, Eur. Phys. J. E 10 (2003) 209–221.
[3] P. Sierro, D. Roux, Structure of a lyotropic lamellar phase under shear, Phys. Rev. Lett. 78 (1997) 1496–1499.
[4] H.J. Wilson, J.M. Rallison, Instability of channel flow of a shear-thinning White–Metzner fluid, J. Non-Newton. Fluid Mech. 87 (1999) 75–96.
[5] P.T. Callaghan, M.E. Cates, C.J. Rofe, J.B.A.F. Smeulders, A study of the spurt effect in wormlike micelles using nuclear magnetic resonance microscopy, J. Phys. II France 6 (1996) 375–393.

[6] R. Larson, The Structure and Rheology of Complex Fluids, Oxford University Press, Oxford, 1999.
[7] M.W. Liberatore, F. Nettesheim, N.J. Wagner, Spatially resolved small-angle neutron scattering in the 1–2 plane: A study of shear-induced phase-separating wormlike micelles, Phys. Rev. E 73 (2006) 020504(R)–020508(R).
[8] V. Schmitt, C.M. Marques, F. Lequeux, Shear-induced phase separation of complex fluids: the role of flow-concentration coupling, Phys. Rev. E 52 (1995) 4009–4015.
[9] L. Kondic, P. Palffy-Muhoray, M.J. Shelley, Models of non-Newtonian Hele-Shaw flow, Phys. Rev. E 54 (1996) 4536–4539.
[10] S. Hess, Structure and nonlinear flow behavior of simple and complex fluids, Int. J. Thermophys. 23 (2002) 905–920.
[11] L.B. Bergström, Nonmodal growth of three-dimensional disturbances on plane Couette–Poiseuille flows, Phys. Fluids 17 (2004) 014105–14115.
[12] Ph. Tordjeman, Saffman–Taylor instability of shear thinning fluids, Phys. Fluids 19 (2007) 118102–118106.
[13] O. Diat, D. Roux, F. Nallet, Layering effect in a sheared lyotropic lamellar phase, Phys. Rev. E 51 (1995) 3296–3299.
[14] S. Manneville, L. Bécu, A. Colin, High-frequency ultrasonic speckle velocimetry in sheared complex fluids, Eur. Phys. J. Appl. Phys. 28 (2004) 361–373.
[15] S. Lerouge, J.P. Decruppe, Correlations between rheological and optical properties of a micellar solution under shear banding flow, Langmuir 16 (2000) 6464–6474.
[16] R.D. Keane, R.J. Adrian, Optimization of particle image velocimeters. I. Double pulsed systems, Meas. Sci. Technol. 1 (1990) 1202–1215.
[17] C. Tropea, A.L. Yarin, J.F. Foss, Springer handbook of experimental fluid mechanics, Springer, 2007.
[18] J. Westerweel, Fundamentals of digital particle image velocimetry, Meas. Sci. Technol. 8 (1997) 1379–1392.
[19] H. Nobach, E. Bodenschatz, Limitations of accuracy in PIV due to individual variations of particle image intensities, Exp. Fluids 47 (2009) 27–38.
[20] J. Westerweel, Theoretical analysis of the measurement precision in particle image velocimetry, Exp. Fluids (2000) 3–12.
[21] J. Westerweel, On velocity gradients in PIV interrogation, Exp. Fluids 44 (2008) 831–842.
[22] R.D. Keane, R.J. Adrian, Y. Zhang, Super-resolution particle imaging velocimetry, Meas. Sci. Technol. 6 (1995) 754–768.
[23] M. Stanislas, K. Okamoto, C.J. Kähler, J. Westerweel, F. Scarano, Main results of the third international PIV challenge, Exp. Fluids 45 (2008) 27–71.
[24] M. Raffel, C.E. Willert, J. Kompenhans, Particle Image Velocimetry: A Practical Guide, Springer, 1998.
[25] P. Joseph, P. Tabeling, Direct measurement of the apparent slip length, Phys. Rev. E 71 (2005) 035303(R)–035307(R).
[26] M. Rossi, R. Lindken, J. Westerweel, Optimization of multiplane μPIV for wall shear stress and wall topography characterization, Exp. Fluids 48 (2010) 211–223.
[27] J. Santiago, S. Wereley, C. Meinhart, D. Beebe, R. Adrian, A particle image velocimetry system for microfluidics, Exp. Fluids 25 (1998) 316–319.
[28] S.W. Stone, C.D. Meinhart, S.T. Wereley, A microfluidic-based nanoscope, Exp. Fluids 33 (2002) 613–619.
[29] T.J. Craven, J.M. Rees, W.B. Zimmerman, Pressure sensor positioning in an electrokinetic microrheometer device. simulations of shear-thinning liquid flows, Microfluid Nanofluid 9 (2010) 559–571.
[30] H.C.H. Bandalusena, W.B. Zimmerman, J.M. Rees, Microfluidic rheometry of a polymer solution by micron resolution particle image velocimetry: a model validation study, Meas. Sci. Technol. 20 (2009) 115404–115413.
[31] A. Lindner, D. Bonn, J. Meunier, Viscous fingering in a shear-thinning fluid, Phys. Fluids 12 (2000) 256–261.
[32] M. Chinaud, T. Delaunay, P. Tordjeman, An experimental study of particle sedimentation by ultrasonic speckle velocimetry, Meas. Sci. Tech. 21 (2010) 055402–55409.
[33] B. Lecordier, D. Demare, L.M.J. Vervisch, J. Rveillon, M. Trinit, Estimation of accuracy of PIV treatments for turbulent flow studies by direct numerical simulation of multiphase flow, Meas. Sci. Tech. 9 (2001) 1382–1391.
[34] R. Perrin, C. Mockett, M. Braza, E. Cid, S. Cazin, A. Sevrain, M. Chassaing, F. Thiele, Joint numerical and experimental investigation of the flow around a circular cylinder at high Reynolds number. In: Particle Image Velocimetry: New developments and recent applications. Topics in Applied Physics, 112, Springer, pp.223-244. ISBN 978-3-540-73527-4.